analytical chemistry

pubs.acs.org/ac

Article

Attomole-Level Multiplexed Detection of Neurochemicals in Picoliter Droplets by On-Chip Nanoelectrospray Ionization Coupled to Mass Spectrometry

Yan Zhang,[‖] Keyin Li,[‖] Yaoyao Zhao, Weihua Shi, Hrishikesh Iyer, Sungho Kim, Christopher Brenden, Jonathan V. Sweedler, and Yurii Vlasov*

Cite This: *Anal. Chem.* 2022, 94, 13804−13809

Read Online

ACCESS | Metrics & More | Article Recommendations

ABSTRACT: While droplet microfluidics is becoming an effective tool for biomedical research, sensitive detection of droplet content is still challenging, especially for multiplexed analytes compartmentalized within ultrasmall droplets down to picoliter volumes. To enable such measurements, we demonstrate a silicon-based integrated microfluidic platform for multiplexed analysis of neurochemicals in picoliter droplets via nanoelectrospray ionization (nESI)-mass spectrometry (MS). An integrated silicon microfluidic chip comprising downscaled 7 μm-radius channels, a compact T-junction for droplet generation, and an integrated nESI emitter tip is used for segmentation of analytes into picoliter compartments and their efficient delivery for subsequent MS detection. The developed system demonstrates effective detection of multiple neurochemicals encapsulated within oil-isolated plugs down to low picoliter volumes. Quantitative measurements for each neurochemical demonstrate limits of detection at the attomole level. Such results are promising for applications involving label-free and small-volume detection for monitoring a range of brain chemicals.

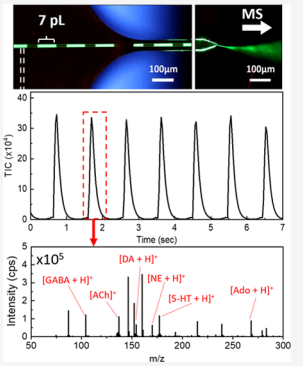

In recent years, there has been growing interest in exploring the ability to generate and process ultrasmall droplets. Reducing droplet volume to a size that is comparable to cells mimics the environment of chemical reactions that take place at single-cell levels[1,2] where diffusion and dilution are limited.[3] For example, volumes in femtoliters to picoliters allow encapsulation of cells or subcellular organelles into a droplet to quantitatively analyze enzyme activity,[4,5] genes,[6] or protein expression.[7,8] Small volumes also enhance mass transfer and mixing of chemicals within droplets[9] while preserving the temporal concentration information. Droplet-based microfluidics has been a powerful tool utilized in multidisciplinary research fields, including single-cell analysis,[10] protein engineering,[11] drug discovery,[12] and also biochemical analysis[13,14] in small-volume droplets. Droplet microfluidics allows for a significant reduction in sample consumption, independent manipulation of individual droplets, and high-throughput analyses.[15]

Quantitative detection of droplet content is an important but challenging feature of droplet microfluidics. Currently, common detection approaches include optical methods,[4,16−20] electrochemical detection,[21,22] nuclear magnetic resonance spectroscopy,[23] and mass spectrometry (MS).[24−26] MS is an attractive detection method for multiplex analysis of biological samples and is especially advantageous for simultaneous measurement of multiple low-concentration neurochemicals in the brain.[27−29] Compared to other techniques, MS has the advantages of label-free detection, high-throughput, and quantitative analysis for complex chemical samples.[30] Two widely used MS techniques applied to droplet content measurement are matrix-assisted laser desorption/ionization (MALDI)[31,32] and electrospray ionization (ESI).[26,33−35] Previously, Bell et al. explored the effects of different oil phases on MALDI-MS analysis of GABA,[36] which laid the groundwork for future analysis of neurochemical systems in low picoliter droplets. Here in this work, we investigated the possibility of hyphenating ultrasmall droplet generation with online ESI-MS analysis.

Conventional ESI emitters are commonly applied to nL−μL droplet volumes.[26,33,34,37,38] For smaller droplets, nanoESI (nESI)-MS[39] is a promising alternative for multiplexed chemical analysis. Because nESI-MS utilizes a narrower spray emitter, resulting in a larger surface/volume ratio and lower flow rates compared to conventional ESI, the approach allows for the use of high-polarity solvents, such as water, and has a higher tolerance to salts.[40] These advantages allow direct

Received: May 31, 2022
Accepted: August 26, 2022
Published: September 27, 2022

https://doi.org/10.1021/acs.analchem.2c02323
Anal. Chem. 2022, 94, 13804−13809

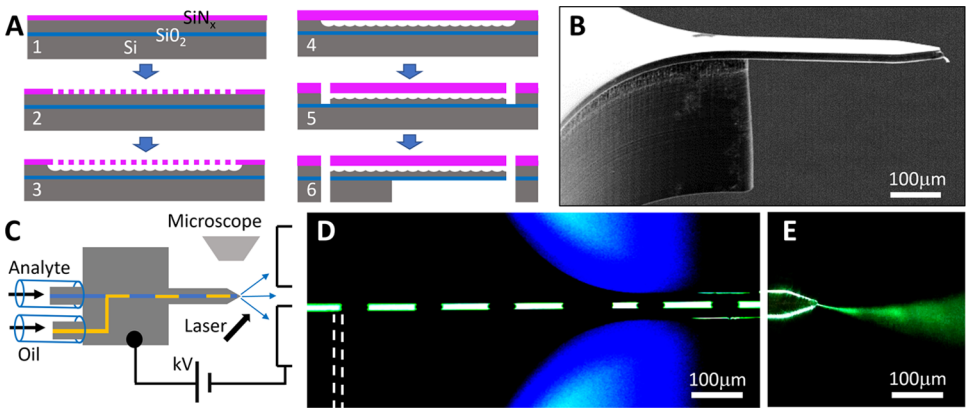

Figure 1. (A) Schematic diagram of the device microfabrication process. Blue: SiO_2, gray: Si, purple: SiNx. (B) Scanning electron microscope photo of the structure of the microfabricated silicon probe tip. (C) Schematics of the packaged chip and the experimental setup. (D) Fluorescence image of on-chip integrated picoliter droplet generation. (E) Single-droplet electrospray plume formation by the integrated nESI emitter.

analysis of biological samples with little sample preparation. nESI-MS also offers enhanced sensitivity and provides the potential for analyzing ultrasmall volumes of analytes.

Although MS is a powerful tool for droplet content detection, it remains challenging to analyze droplets in the low picoliter regime. Most of the previous studies using droplet microfluidics coupled with nESI-MS worked with droplets in the range of hundreds of picoliters to nanoliter volumes.[26,33,34,37] The smallest droplet volume analyzed by nESI-MS reported thus far was 65 pL generated on polydimethylsiloxane chips connected to commercial nESI emitters.[41] Various experimental conditions hinder the further reduction of droplet volumes that are detectable by nESI-MS analysis. First, to achieve efficient ionization for low picoliter-scale volumes, droplets need to be generated and sprayed at lower flow rates, even down to nL/min, to maximize the ionization efficiency[42−44] and match the scan speed of spectrometers.[45] Other properties, including surface tension,[46] carrier oils, sample concentration, and electrospray potentials,[47] also have a strong influence on the droplet generation, spray stability, and ionization efficiency of analytes[48] in nESI-MS.[40] In addition, most droplet generators reported previously have been connected to external ESI emitters, which may introduce dead volumes and sample loss in the connecting tubes.

In this work, we developed a miniaturized silicon microfluidic platform that monolithically integrates a T-junction droplet generator and a miniaturized ESI emitter to effectively perform quantitative, multiplexed analysis of neurochemicals in picoliter volume oil-isolated aqueous plugs by nESI-MS. To investigate the quantitative analysis and multiplexed detection ability of this system, plugs containing multiple neurochemical standards were generated on-chip prior to MS detection. The results demonstrated the ability of our integrated miniaturized silicon microfluidic platform for multiplexed and sensitive detection of picoliter compartmentalized chemicals.

EXPERIMENTAL SECTION

Reagents. Fluorescein, fluorinert FC-40, dopamine hydrochloride, acetylcholine chloride, DL-norepinephrine hydrochloride, serotonin hydrochloride, adenosine (Ado), and γ-aminobutyric acid (GABA) were purchased from Sigma-Aldrich (St. Louis, MO). Solutions were prepared with HPLC-grade water. For the multiplexing detection experiment, a master solution of neurochemical standards was prepared by dissolving six neurochemicals into deionized (DI) water, including 25 μM Ado, 50 μM acetylcholine (ACh), 50 μM dopamine (DA), 125 μM norepinephrine (NE), and 125 μM serotonin (5-HT). Then, this mixture was diluted into a series of concentrations while GABA was kept at 25 μM in all mixtures.

Chip Fabrication. Although silicon-based microfabrication techniques, including surface micromachining and bulk micromachining methods,[49] have been demonstrated to successfully create probe shank and integrated microfluidics channels, the performance demand for our probe requires greater attention to the fabrication process.[50] First, the probe must be electrically conductive, with the cross-section of the probe tip no larger than 20 × 50 μm^2, so that the electrical field can be focused and strengthened at the tip to enable efficient nESI. Second, the embedded microfluidic channel diameter should not exceed 15 μm to ensure picoliter droplet generation and maintenance of the mechanical stability of the suspended probe tip. Next, the microfluidic channels should be visible so that the droplet-generation dynamics can be characterized using conventional fluorescence microscopy. Furthermore, the targeted probe aims at monolithic integration of all microfluidics networks for droplet-on-demand generation devices, and the nESI emitter module, onto the miniaturized silicon probe so that the device can be conveniently coupled to a mass spectrometer for analyte detection.

To achieve the performance requirements for the probe as noted above, a specially designed process for probe microfabrication was developed, as shown in Figure 1A, which is based on our recent exploration work on silicon microfluidic platform that enables the separation of oil and aqueous phases during electrospray.[50] The fabrication of the neural probes starts with a degreased double-side polished silicon-on-insulator (SOI) wafer. The choice of SOI wafer should accommodate all requirements for the probe system design. The device thickness determines the probe shank cross-section size, and handle wafer thickness should be matched with the plumbing capillary inner diameter for packaging. The wafer should preferably also be heavily doped to enable the application of high voltage onto the integrated electrospray tip. The metrics of the SOI wafer we selected are as follows: P/B doped; device layer thickness: 15 ± 1 μm; handle wafer thickness: 450 ± 10 μm; orientation: ⟨100⟩; buried thermal

https://doi.org/10.1021/acs.analchem.2c02323
Anal. Chem. 2022, 94, 13804−13809

oxide thickness: 0.5 μm; device layer resistivity: 0.001−0.005 Ω·cm; and handle wafer resistivity: 1−20 Ω·cm.

The first fabrication step (Figure 1A.1) was the deposition of a 300 nm silicon nitride (SiNx) layer onto a device layer of SOI wafer (4-11294, Ultrasil Corporation, Hayward, CA) by plasma-enhanced chemical vapor deposition (PECVD). The fluidics channels were subsequently formed by XeF_2 isotropic etching of the silicon layer through a series of μm-size holes defined by direct laser writing lithography (Figure 1A.2) and plasma etching through this overcladding SiNx hard mask (Figure 1A.3). The fabricated channels were then sealed by deposition of 4 μm-thick silicon nitride by PECVD (Figure 1A.4). In this way, after sealing, the channel cover is transparent, enabling direct observation of droplet fluidics dynamics via fluorescence microscopy. Next, the perimeter of the chip and the ESI emitter was defined by aligned lithography, and the SiNx cover was etched away by the inductively coupled plasma-reactive ion etching (ICP-RIE) to expose the bare silicon surface. This was followed by deep reactive ion etching (DRIE) all of the way through the silicon device layer until stopped by the buried thermal oxide (Figure 1A.5). Last aligned lithography step on the wafer backside defined the perimeter of the chip and the nESI emitter. Backside DRIE was used to etch away the underlying handle silicon layer to release suspended ESI emitter cantilevers (Figure 1A.6). The structure of the microfabricated silicon probe is shown in Figure 1B.

The fabricated chip is released from the wafer and is packaged to provide fluidic and electrical interfaces (Figure 1C). To interface with external microfluidic pumps, the 450 × 450 μm^2 silicon stubs on the chip base are shaped to fit with 15 cm-long silica capillaries (Polymicro TSP530700, 650 μm ID). UV curable resin (Norland Products, NOA 68T) is sealing the stub−capillary junction. The silicon microfabrication platform enables doping of the silicon device layer, thus providing low resistivity electrical connection (0.005 Ω·cm). Hence the voltage applied at the chip base via copper tape (Figure 1C) glued with conductive adhesive (MG Chemicals 8331D) is effectively applied to the suspended nESI tip enabling electrospray ionization.

Offline Characterization of Flow Segmentation and Electrospray Visualization. A pressure pump (Flow-EZ Module, LU_FEZ_7000, Fluigent, North Chelmsford, MA) was used to control the flow rate of the oil phase (Fluorinert FC-40), while a syringe pump (Harvard Apparatus 11 Pico Plus Elite, Holliston, MA) equipped with 250 μL syringe (Gastight, 1700 Series) was used for flow control of the aqueous phase (1 mM fluorescein in DI water). An inverted fluorescence microscope (Olympus IX73, Shinjuku, Japan) equipped with a fast video camera (Canon EOS Rebel T7i, Melville, NY) was used to observe fluidic flows and droplet formation.

As fabricated, the internal surfaces of microfluidic channels are covered with a native silicon oxide layer and potentially by a SiNx layer, making them hydrophilic. The contact angle of the aqueous/oil interface as measured from the meniscus in Figure 1D is about 40°. Therefore, strictly speaking, the aqueous phase (bright areas in Figure 1D, with fluorescein) is a continuous phase that is segmented into individual aqueous plugs with dispersed oil phase droplets (dark areas in Figure 1D, no fluorescein).

Knowing the cross-section of the microfluidic channels, the linear extent of the plugs/droplets along the channel length, and the meniscus angles, the plugs/droplets volumes can be measured directly from fluorescent images (Figure 1D) to quantify the frequency and volumes of segmented flows.

To visualize the electrospray formation, a 3 mW 532 nm laser light was collimated and projected onto the nESI emitter nozzle and the electrosprayed plume (Figure 1E).

nESI−MS Interface. The samples were analyzed using an ultrahigh-resolution quadrupole time-of-flight maXis 4G tandem mass spectrometer (Bruker Corporation, Billerica, MA) in positive ion mode. To couple our fabricated device to MS detection, the silicon chip was placed on a micromanipulator, allowing movement in three dimensions, which was used to move the silicon chip into the appropriate position in front of the mass spectrometer with a 2 mm gap between the ESI emitter and the MS inlet (Figure 1C). The oil-segmented picoliter aqueous plugs were delivered to the chip outlet with an integrated nESI emitter at a flow rate below 10 nL/min (Figure 1D). Application of electric potential of 1.55−2 kV between the chip base and the entrance plate of the MS (Figure 1C) results in the formation of a narrow cone-jet electrospray plume (Figure 1E). The voltages were slightly adjusted for samples with different chemical concentrations to achieve stable droplet generation and maximize ESI intensity. For the multiplexing detection experiment, we measured five neurochemical standard mixtures with various dilution ratios. All measurements shown here were done with a single silicon chip. In between each measurement, we flushed the channels for at least 4 hours to alleviate possible contamination from residual solution. OriginPro 2021b SR2 (OriginLab Corporation, Northampton, MA) was used for data processing, peak detection, peak area calculation, and linear fitting of calibration curves.

RESULTS AND DISCUSSION

To examine the multiplexed detection ability of our system, we prepared multiplexed mixture standards containing six neurochemicals: GABA, ACh, DA, NE, 5-HT, and Ado. Oil-isolated plugs containing these chemical mixtures were generated on-chip and subsequently delivered to MS detection via an integrated nESI emitter. As shown in Figure 2A, the total ion chromatogram (TIC) trace shows consistent, stable peak intensity (RSD < 5%) at a constant frequency. Each peak corresponds to a distinct electrosprayed aqueous segment containing chemical mixtures, with its corresponding extracted mass spectrum shown in Figure 2B. The mass spectrum extracted from the peaks validated the successful simultaneous detection of all six neurochemicals.

The drop in TIC intensity between neighboring peaks corresponds to the oil phase being eluted from the electrospray emitter. Since the fabricated microfluidic channels are hydrophilic, the continuity of the aqueous phase might result in a carry-over of the analyte content from one plug to another. As can be seen in Figure 2C, the mass spectrum extracted from the bottom of the TIC traces shows that the signal intensity detected between the peaks was approximately 3 orders of magnitude lower, close to the background noise level in the blank sample, indicating minimal carry-over. A detailed comparison of EIC peaks for individual analytes at the TIC peak maximum (Figure 2B) and minimum (Figure 2C) confirms that the carry-over between neighboring aqueous plugs is suppressed by about 3 orders of magnitude for all six analytes measured. These results confirm the multiplexing capability of our system.

https://doi.org/10.1021/acs.analchem.2c02323
Anal. Chem. 2022, 94, 13804−13809

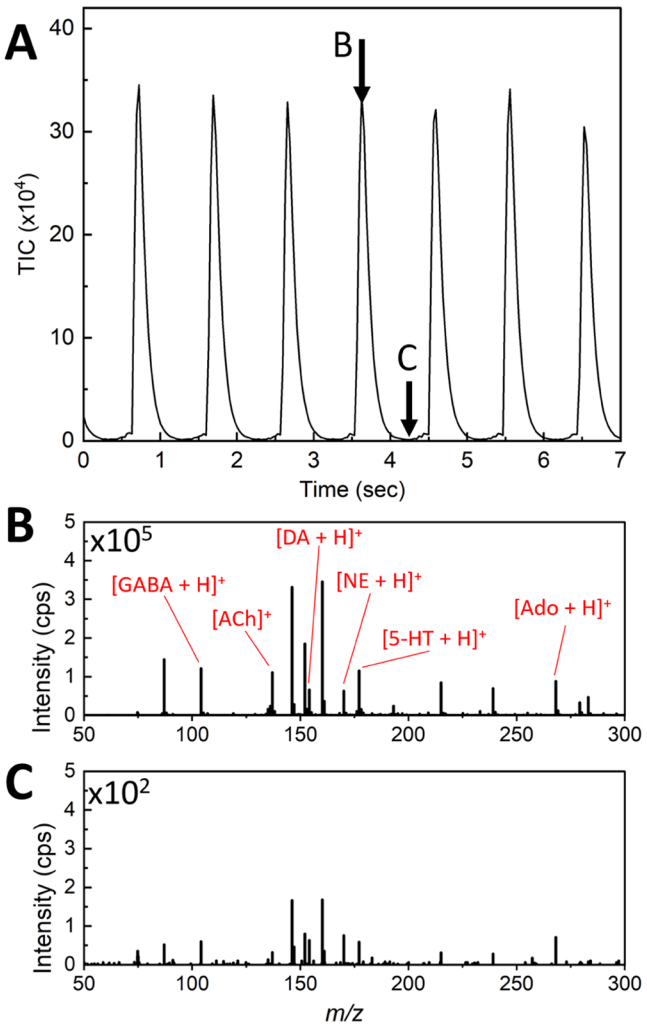

Figure 2. (A) TIC trace of the multiplexed standard mixture. The arrows indicate spectrum (B) extracted from the apex of the peak and spectrum (C) extracted from the base of the peak.

We then tested the concentration-based detection response of segmented chemicals to investigate its limit of detection (LOD). To measure concentration sensitivity for segmented flows, it is critical to ensure constant plug volume throughout the measurement cycle. Calibration of droplet generation (Figure 3A) demonstrates that the device was able to work in a wide range of water/oil flow rate ratios while the generated aqueous plug volumes are maintained within a narrow range of 4−7 pL that would alleviate the influence of potential variability of analyte volumes on MS analysis.

The samples were segmented into 7 pL plugs isolated by inert FC-40 oil and transferred to the mass spectrometer via our integrated nESI tip, with corresponding extracted ion chromatogram (EIC) recorded. Here, we take Ado in the chemical mixtures as an example to demonstrate the quantitative detection ability of our system. EIC intensity for Ado at different concentrations is shown in Figure 3B,C with *y*-axis multipliers at the upper left corner of each plot. At higher concentrations (1−25 μM), aqueous phase peaks are detectable and well resolved (Figure 3B). Lower concentrations down to 0.1 μM and blank samples were also tested (Figure 3C). Although a trace of periodic peaks of Ado is still visually detectable by EIC at 0.1 μM, the low intensity of peaks and interference from the background noise make it difficult to determine the boundaries of each droplet peak. To discern EIC peaks corresponding to each aqueous plug at 0.1 μM, TIC trace, where peaks were discernible, was used to pinpoint the time windows of each plug peak. As the concentration of GABA was kept constant in all samples, for each sample tested, we fine-tuned the applied voltage (within 15%) to achieve the optimal GABA EIC intensity. While the electric field is mostly applied to the highly doped silicon device layer, the voltage drop at the electrolytic fluid flow can potentially produce additional electro-osmotic drag that affects the actual flow rates within the device, which might explain the slight differences in detected droplet frequencies among each test (Figure 3B,C). However, Figure 3A calibration indicates that slight changes in the flow rate will not change the aqueous plug volume significantly. Therefore, we used 7 pL as an estimation of the plug volumes in each test.

To quantify the LOD of our system, 80 consecutive aqueous plug peaks were extracted from each concentration test to generate a calibration curve of peak area against analyte concentration. While some scattering of the data is observed, the linear fitting can well describe the measurements with a slope of 1.68 ± 0.26 (R^2 = 0.93, Pearson coefficient P = 0.97), as shown in Figure 3D. The LOD was calculated as ($\text{Mean}_{\text{blank}}$ + 3 × $\text{Standard\_Deviation}_{\text{blank}}$ − intercept) /slope. For Ado, the concentration LOD was calculated to be 0.2 μM, which corresponds to 1.4 amol of analyte in 7 pL plugs at a 99% confidence level. These results demonstrate the ability of our system to perform sensitive detection of neurochemical standards in picoliter aqueous plugs.

To quantify the LODs of each analyte within the mixture, LOD analysis of plugs containing varying concentrations of the

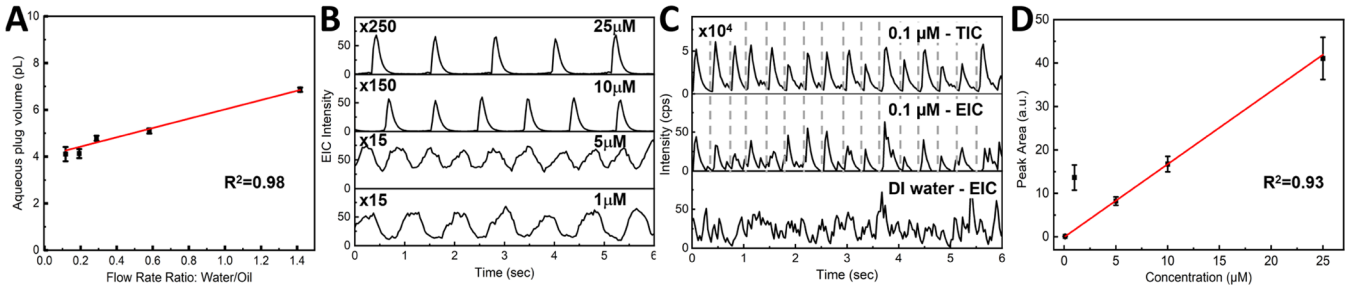

Figure 3. (A) Calibrated dependence of generated aqueous plug volume against water/oil flow rate ratio. (B) EIC intensity of Ado signal of varying concentrations in 7 pL plugs. From top to bottom: 25, 10, 5, and 1 μM. (C) From top to bottom: TIC intensity of 0.1 μM Ado, EIC intensity of 0.1 μM Ado, and EIC intensity of blank sample. (D) Calibration curve of detected EIC peak area vs corresponding chemical concentration of Ado within plugs.

https://doi.org/10.1021/acs.analchem.2c02323
Anal. Chem. 2022, 94, 13804−13809

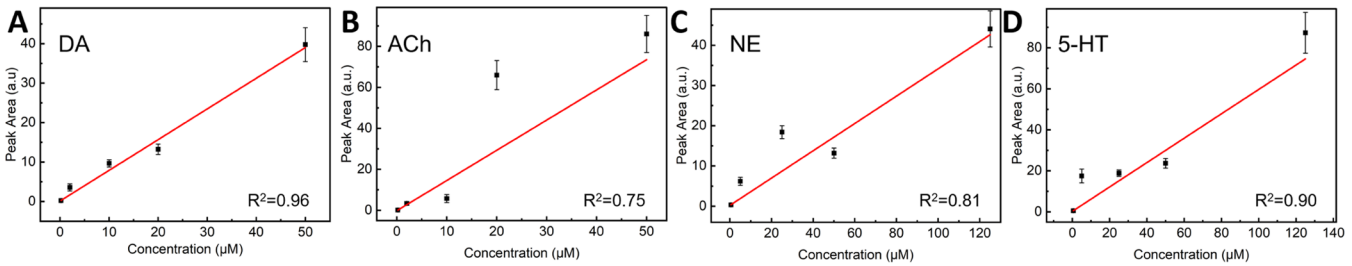

Figure 4. Calibration curves of peak area against analyte concentration for (A) dopamine (DA), (B) acetylcholine (ACh), (C) norepinephrine (NE), and (D) serotonin (5-HT). Error bars represent standard deviations.

analyte mixture was performed. Eighty consecutive plugs were selected from each concentration test for the calculation of peak areas and their standard deviation (SD). Calibration curves were generated for four analytes from the multiplexing solutions (Figure 4). LODs were calculated to be 0.28 μM for DA, 0.56 μM for ACh, 0.86 μM for NE, and 3.54 μM for 5-HT, corresponding to 2.0 amol DA, 3.9 amol ACh, 6.0 amol NE, and 24.8 amol 5-HT in 7 pL plug volumes with a 99% confidence level (Table 1). While robust, the calibration data

Table 1. LODs of Individual Neurochemicals within a Single Droplet

chemicals	m/z	LOD (amol)	R^2	Pearson
Ado	268.1	1.4	0.93	0.97
DA	154.09	2.0	0.96	0.98
ACh	146.12	3.9	0.75	0.86
NE	170.07	6.0	0.81	0.90
5-HT	177.1	24.8	0.90	0.95

show significant scattering, in an analyte-specific manner. This may be due to the slight differences in the ionization efficiency of each analyte as the electrical potentials for different samples were adjusted based on the EIC intensity of GABA. Another possible explanation is the interactions of these analytes with surfaces or fluids during sample loading or transfer, which will be investigated in future experiments. This result demonstrates the ability of our system to perform multiplex quantitative analysis in sub-10 pL droplets with amol-level LODs.

CONCLUSIONS

We developed a silicon platform technology that enables on-chip integration of downscaled microfluidic channels, a miniaturized T-junction droplet generator, and an nESI emitter to efficiently deliver and detect compartmentalized picoliter neurochemicals by MS. The integrated silicon nESI platform was validated for sensitive detection of multiplexed neurochemicals encapsulated within picoliter-scale oil-isolated compartments. Quantitative measurements of detection sensitivity for each chemical of various concentrations demonstrate LODs at the attomole level for DA, ACh, NE, 5-HT, and Ado. Ado showed the best LOD of 1.4 amol, demonstrating the potential of the integrated micromachined nESI emitter tips for biomolecular analysis and laying a foundation for further adoption in different applications, such as monitoring the highly diverse brain chemicals, the study of organic synthesis, and measuring metabolites produced by microorganisms.

AUTHOR INFORMATION

Corresponding Author

Yurii Vlasov − *Department of Electrical and Computer Engineering, University of Illinois Urbana Champaign, Urbana, Illinois 61801, United States; Department of Bioengineering, University of Illinois Urbana Champaign, Urbana, Illinois 61801, United States;* orcid.org/0000-0002-5864-3346; Email: yvlasov@illinois.edu

Authors

Yan Zhang − *Department of Electrical and Computer Engineering, University of Illinois Urbana Champaign, Urbana, Illinois 61801, United States*

Keyin Li − *Department of Chemistry and the Beckman Institute, University of Illinois Urbana Champaign, Urbana, Illinois 61801, United States*

Yaoyao Zhao − *Department of Chemistry and the Beckman Institute, University of Illinois Urbana Champaign, Urbana, Illinois 61801, United States*

Weihua Shi − *Department of Electrical and Computer Engineering, University of Illinois Urbana Champaign, Urbana, Illinois 61801, United States*

Hrishikesh Iyer − *Department of Electrical and Computer Engineering, University of Illinois Urbana Champaign, Urbana, Illinois 61801, United States*

Sungho Kim − *Department of Electrical and Computer Engineering, University of Illinois Urbana Champaign, Urbana, Illinois 61801, United States;* orcid.org/0000-0002-7838-9744

Christopher Brenden − *Department of Bioengineering, University of Illinois Urbana Champaign, Urbana, Illinois 61801, United States*

Jonathan V. Sweedler − *Department of Chemistry and the Beckman Institute, University of Illinois Urbana Champaign, Urbana, Illinois 61801, United States;* orcid.org/0000-0003-3107-9922

Complete contact information is available at: https://pubs.acs.org/10.1021/acs.analchem.2c02323

Author Contributions

[‖]Y.Z. and K.L. contributed equally to this paper. The manuscript was written through contributions of all authors. All authors have given approval to the final version of the manuscript.

Notes

The authors declare no competing financial interest.

ACKNOWLEDGMENTS

This project was supported in part by the National Institute of Neurological Disorders and Stroke (NINDS) under Award

Nos. UF1NS107677 and RF1NS126061 and the National Institute on Drug Abuse (NIDA) under Award No. P30DA018310. The content is solely the responsibility of the authors and does not necessarily represent the official views of the National Institutes of Health.

REFERENCES

(1) Chiu, D. T. *TrAC, Trends Anal. Chem.* **2003**, *22*, 528−536.
(2) Gadd, J. C.; Kuyper, C. L.; Fujimoto, B. S.; Allen, R. W.; Chiu, D. T. *Anal. Chem.* **2008**, *80*, 3450−3457.
(3) Song, H.; Tice, J. D.; Ismagilov, R. F. *Angew. Chem., Int. Ed.* **2003**, *42*, 768−772.
(4) He, M.; Edgar, J. S.; Jeffries, G. D. M.; Lorenz, R. M.; Shelby, J. P.; Chiu, D. T. *Anal. Chem.* **2005**, *77*, 1539−1544.
(5) Gu, S.-Q.; Zhang, Y.-X.; Zhu, Y.; Du, W.-B.; Yao, B.; Fang, Q. *Anal. Chem.* **2011**, *83*, 7570−7576.
(6) Zeng, Y.; Novak, R.; Shuga, J.; Smith, M. T.; Mathies, R. A. *Anal. Chem.* **2010**, *82*, 3183−3190.
(7) Huebner, A.; Srisa-Art, M.; Holt, D.; Abell, C.; Hollfelder, F.; deMello, A. J.; Edel, J. B. *Chem. Commun.* **2007**, 1218−1220.
(8) Joensson, H. N.; Samuels, M. L.; Brouzes, E. R.; Medkova, M.; Uhlén, M.; Link, D. R.; Andersson-Svahn, H. *Angew. Chem. Int. Ed.* **2009**, *48*, 2518−2521.
(9) Song, H.; Ismagilov, R. F. *J. Am. Chem. Soc.* **2003**, *125*, 14613−14619.
(10) Matuła, K.; Rivello, F.; Huck, W. T. S. *Adv. Biosyst.* **2020**, *4*, No. 1900188.
(11) Weng, L.; Spoonamore, J. E. *Micromachines* **2019**, *10*, 734.
(12) Wang, Y.; Chen, Z.; Bian, F.; Shang, L.; Zhu, K.; Zhao, Y. *Expert Opin. Drug Discovery* **2020**, *15*, 969−979.
(13) Gao, D.; Jin, F.; Zhou, M.; Jiang, Y. *Analyst* **2019**, *144*, 766−781.
(14) Petit-Pierre, G.; Colin, P.; Laurer, E.; Déglon, J.; Bertsch, A.; Thomas, A.; Schneider, B. L.; Renaud, P. *Nat. Commun.* **2017**, *8*, No. 1239.
(15) Shang, L.; Cheng, Y.; Zhao, Y. *Chem. Rev.* **2017**, *117*, 7964−8040.
(16) Kim, S.-H.; Shim, J. W.; Yang, S.-M. *Angew. Chem., Int. Ed.* **2011**, *50*, 1171−1174.
(17) Chan, K. L. A.; Niu, X.; deMello, A. J.; Kazarian, S. G. *Anal. Chem.* **2011**, *83*, 3606−3609.
(18) Beneyton, T.; Wijaya, I. P. M.; Postros, P.; Najah, M.; Leblond, P.; Couvent, A.; Mayot, E.; Griffiths, A. D.; Drevelle, A. *Sci. Rep.* **2016**, *6*, No. 27223.
(19) Konry, T.; Golberg, A.; Yarmush, M. *Sci. Rep.* **2013**, *3*, No. 3179.
(20) Toprakcioglu, Z.; Challa, P. K.; Morse, D. B.; Knowles, T. *Sci. Adv.* **2020**, *6*, No. eaay7952.
(21) Liu, S.; Gu, Y.; Le Roux, R. B.; Matthews, S. M.; Bratton, D.; Yunus, K.; Fisher, A. C.; Huck, W. T. S. *Lab Chip* **2008**, *8*, 1937−1942.
(22) Gu, S.; Lu, Y.; Ding, Y.; Li, L.; Zhang, F.; Wu, Q. *Anal. Chim. Acta* **2013**, *796*, 68−74.
(23) Lin, Y.; Schiavo, S.; Orjala, J.; Vouros, P.; Kautz, R. *Anal. Chem.* **2008**, *80*, 8045−8054.
(24) Baker, C. A.; Roper, M. G. *Anal. Chem.* **2012**, *84*, 2955−2960.
(25) Gasilova, N.; Yu, Q.; Qiao, L.; Girault, H. H. *Angew. Chem. Int. Ed.* **2014**, *53*, 4408−4412.
(26) Smith, C. A.; Li, X.; Mize, T. H.; Sharpe, T. D.; Graziani, E. I.; Abell, C.; Huck, W. T. S. *Anal. Chem.* **2013**, *85*, 3812−3816.
(27) Zheng, X.; Kang, A.; Dai, C.; Liang, Y.; Xie, T.; Xie, L.; Peng, Y.; Wang, G.; Hao, H. *Anal. Chem.* **2012**, *84*, 10044−10051.
(28) Song, P.; Mabrouk, O. S.; Hershey, N. D.; Kennedy, R. T. *Anal. Chem.* **2012**, *84*, 412−419.
(29) Hanrieder, J.; Zetterberg, H.; Blennow, K. MALDI Imaging Mass Spectrometry: Neurochemical Imaging of Proteins and Peptides. In *Neuroproteomics*, Li, K. W., Ed.; Springer New York: New York, NY, 2019; pp 179−197.
(30) Tillmaand, E. G.; Sweedler, J. V. *Microphysiological Syst.* **2018**, *1*, 1.
(31) Sun, W.-H.; Wei, Y.; Guo, X.-L.; Wu, Q.; Di, X.; Fang, Q. *Anal. Chem.* **2020**, *92*, 8759−8767.
(32) Mesbah, K.; Thai, R.; Bregant, S.; Malloggi, F. *Sci. Rep.* **2017**, *7*, No. 6756.
(33) Ngernsutivorakul, T.; Steyer, D. J.; Valenta, A. C.; Kennedy, R. T. *Anal. Chem.* **2018**, *90*, 10943−10950.
(34) Su, Y.; Zhu, Y.; Fang, Q. *Lab Chip* **2013**, *13*, 1876−1882.
(35) Huang, C.-M.; Zhu, Y.; Jin, D.-Q.; Kelly, R. T.; Fang, Q. *Anal. Chem.* **2017**, *89*, 9009−9016.
(36) Bell, S. E.; Park, I.; Rubakhin, S. S.; Bashir, R.; Vlasov, Y.; Sweedler, J. V. *ACS Meas. Sci. Au* **2021**, *1*, 147−156.
(37) Diefenbach, X. W.; Farasat, I.; Guetschow, E. D.; Welch, C. J.; Kennedy, R. T.; Sun, S.; Moore, J. C. *ACS Omega* **2018**, *3*, 1498−1508.
(38) Kertesz, V.; Vavrek, M.; Freddo, C.; Van Berkel, G. J. *Int. J. Mass Spectrom.* **2019**, *437*, 17−22.
(39) Schmidt, A.; Karas, M.; Dülcks, T. *J. Am. Soc. Mass Spectrom.* **2003**, *14*, 492−500.
(40) Gross, J. H., *Mass Spectrometry: A Textbook*; Springer Science & Business Media, 2006.
(41) Steyer, D. J.; Kennedy, R. T. *Anal. Chem.* **2019**, *91*, 6645−6651.
(42) Page, J. S.; Kelly, R. T.; Tang, K.; Smith, R. D. *J. Am. Soc. Mass Spectrom.* **2007**, *18*, 1582−1590.
(43) Heemskerk, A. A. M.; Busnel, J.-M.; Schoenmaker, B.; Derks, R. J. E.; Klychnikov, O.; Hensbergen, P. J.; Deelder, A. M.; Mayboroda, O. A. *Anal. Chem.* **2012**, *84*, 4552−4559.
(44) El-Faramawy, A.; Siu, K. W. M.; Thomson, B. A. *J. Am. Soc. Mass Spectrom.* **2005**, *16*, 1702−1707.
(45) Payne, E. M.; Holland-Moritz, D. A.; Sun, S.; Kennedy, R. T. *Lab Chip* **2020**, *20*, 2247−2262.
(46) Kageyama Kaneshima, A.; Motoyama, A.; Takayama, M. *Mass Spectrom.* **2019**, *8*, A0077.
(47) Peretzki, A. J.; Schmidt, S.; Flachowsky, E.; Das, A.; Gerhardt, R. F.; Belder, D. *Lab Chip* **2020**, *20*, 4456−4465.
(48) Bruins, A. P. *J. Chromatogr. A* **1998**, *794*, 345−357.
(49) Ziaie, B.; Baldi, A.; Lei, M.; Gu, Y.; Siegel, R. A. *Adv. Drug Delivery Rev.* **2004**, *56*, 145−172.
(50) Zhang, Y.; Kim, S.; Shi, W.; Zhao, Y.; Park, I.; Brenden, C.; Iyer, H.; Jha, P.; Bashir, R.; Sweedler, J. V.; Vlasov, Y. *Lab Chip* **2021**, *22*, 40−46.

https://doi.org/10.1021/acs.analchem.2c02323
Anal. Chem. 2022, 94, 13804−13809